Ultrafast-Laser-Processed Zirconia and its Adhesion to Dental Cement

Niko BÄRSCH*, Stephan BARCIKOWSKI* and Klaus BAIER**

* *Laser Zentrum Hannover e.V., Hollerithallee 8, Hannover, Germany*
E-mail: N.Baersch@lzh.de
** *Kugler GmbH, Heiligenberger Str. 100, Salem, Germany*

Hard zirconia ceramic in its hot-isostatically pressed constitution can be machined precisely and reproducibly using ultrafast lasers. However, the pulse overlap turns out to be of significant influence on the resulting surface quality. This can be traced back to particulate process emission from the workpiece surface that influences subsequent pulses in the case of large pulse overlapping and can even agglomerate to debris layers above the processed surface. Measurements of particle emission indicate that 90 % of the ablated particulate material consists of nanoparticles, raising the demands on safe machine housing and suction measures. To produce all-ceramic dental crowns directly from sintered blanks without thermal damage or tool wear, a processing station, including a femtosecond laser system, has been designed based on high necessary processing dynamics and considering safety aspects.

Regarding its adhesion to dental cement, Y-TZP has deficits compared to dentin. The fixation between cement and Y-TZP surfaces can be improved by artificial microstructures, added to the inner surface of laser-processed dental crowns in a final step during ultrafast-laser-based manufacturing. Such microstructures have been evaluated by adhesion measurements between ceramic and cement that were based on shear and tensile strength tests, taking into consideration limit values from numeric simulations.

DOI: 10.2961/jlmn.2008.02.0004

Keywords: femtosecond laser, microstructures, ceramics, zirconia, adhesion, dental prostheses

1. Introduction

All-ceramic dental crowns from yttrium-stabilised tetragonal zirconia polycrystal (Y-TZP) are the cutting-edge solution for dental restorations, with regard to cosmetic aspects as well as mechanical durability. The nanocrystalline material in its final hot-isostatically pressed constitution can be machined with femtosecond lasers as the most precise, damage-free, and wear-free tool for micromachining. Dental crowns are intended to be shaped in a fully automated process according to CAD geometries that are generated from patients' dentitions [1].

Fixation between crowns and cement remains a weak point. Regarding its adhesion to dental cement, Y-TZP has disadvantages compared to natural dentin. This is due to mechanical bonding to dentin tubules – hollow perpendicular tubes travelling from the pulp to the enamel undersurface – to which cements are mechanically locked at the surface of a dental stump. This raises the question whether the fixation between cement and Y-TZP surfaces could be improved similarly by artificial microstructures. Such structures could be added to the inner surface of laser-processed dental crowns in a final step after ultrafast-laser-based manufacturing.

2. Ultrafast laser machining of Y-TZP

2.1 Processing strategy

For the complete shaping of dental crowns from ceramic blanks (measuring about 500 to 1000 mm³), about 70 % of the bulk material needs to be removed efficiently and without inducing thermal load or residual stress. A new generation of femtosecond lasers with average powers up to 15 W will realize this efficient ablation without thermal and mechanical influence on the bulk material. This is one of the main advantages compared to mechanical milling, which involves strong tool wear and is known to reduce the strength of the samples [1, 2].

To achieve this, complete blocks will be cut of the ceramic part during a first stage of processing as visualised in Figure 1 [2]. This strategy is designed to significantly save laser machining time and is the main requirement to produce dental restorations cost-effectively from full blocks. According to calculations from CAD simulation, it should decrease the machining time by a factor greater than ten and lead to processing times with an average of one hour, depending on size and complexity of the crowns.

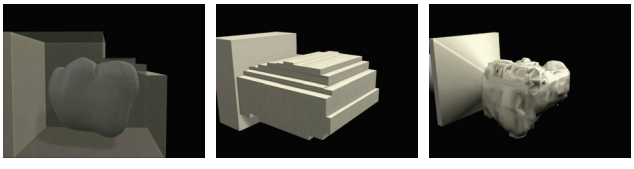

Figure 1: Strategy to remove large amounts of material

In a second processing step, material is removed smoothly using low laser fluences to meet the exact restoration shape. To predict ablation rates during the machining of Y-TZP, depth measurements have been made which are summarised in Figure 2. For a large set of values, ablation depths were measured using different working distances,

including large spot diameters for every applied pulse energy. This helps to compensate possible inaccuracies from beam radius and M² measurements to obtain higher accuracies than in former investigations. The ablation threshold amounts to 1 J/cm², with maximum ablation exceeding 600 nm per pulse at a fluence of 100 J/cm². Besides a good scalability of the ablation depths, the strictly logarithmic increase indicates that thermal effects are mainly avoided. This ensures high quality ablation during femtosecond laser machining, even at high laser fluences, and allows removing predictable amounts of material reproducibly.

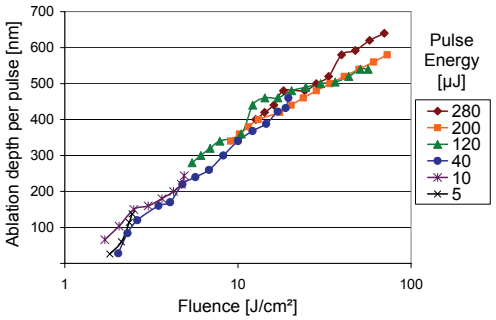

Figure 2: Y-TZP ablation rates using 150 fs pulses

Figure 3 shows cuts of high quality both for high and low pulse energies. Using the applied parameters, femtosecond pulses produce deep cuts in Y-TZP that are optimised with regard to edge qualities for both laser power regimes. However, to generate deep cuts with higher efficiency, a stronger focussing and lower pulse overlapping will be applied for the fast removal of material blocks during the first stage of dental crown machining.

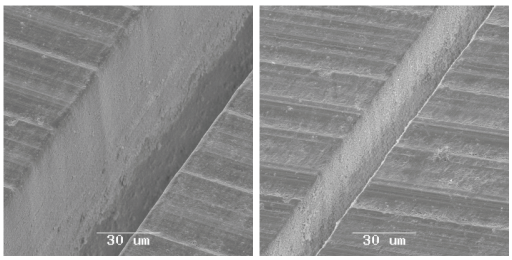

Figure 3: High quality sample lines processed in 16 iterations using a fluence of 80 J/cm² (P = 800 mW) at 10 mm/min (left) and a fluence of 60 J/cm² (P = 50 mW) at 40 mm/min (right)

One of the most relevant parameters is the ratio of pulse overlapping, which is the ablation diameter in relation to pulse-to-pulse distance (the latter resulting from pulse repetition and linear feed rate). The influence of the pulse overlap on ablation quality is shown impressively in Figure 4, in which only the processing speed (feed rate) has been changed. In the given case, the lines were generated in a single step, using two similar processes with huge pulse overlaps (98.5 % on the left, 97 % on the right), and showing an extremely different resulting ground surface quality.

Such differences in the ablation result cannot be explained by ray tracing approaches. It is known that especially for crystalline material and linear polarisations, slight initial inhomogeneities can be amplified during subsequent pulses, if the reflection behaviour of processed surfaces changes disproportionately [16, 17]. However, huge differences in quality are only reported and traceable in cases of changing polarisation. Instead, the effect shown in Figure 4 can be explained with the behaviour of the ablated particulate material, called debris, which influences the ablation process during subsequent laser pulses. The fact that debris plays an important role during ultrafast laser processing of zirconia can be verified by emission measurements and an analysis of processed surfaces.

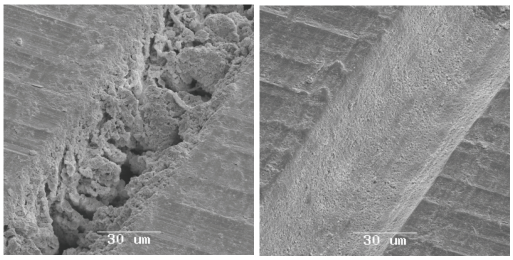

Figure 4: Sample lines processed using a fluence of 80 J/cm² (P = 800 mW), at a pulse overlap of 98.5 % (left) and 97 % (right)

2.2 Particulate process emission

The generation of particles during the ablation process is relevant for two major aspects: safety issues at the workplace, and the ablation quality and efficiency.

During ultrashort-pulsed laser ablation, nanoparticles are emitted from the processed surface, which can bear hazards to the operator of a laser processing station, depending on material, number, and especially size of the particles [5, 6, 7]. Possible hazards are generally discussed when particle sizes are in the range of tens to hundreds of nanometers, because these particles are highly respirable and can pass common natural barriers, and the comparatively large specific surface increases their reactivity [8, 9].

In the course of the investigations on fs laser ablation of Y-TZP, particulate emission from the processed surface was analysed online using an electrical low-pressure impactor (ELPI, Decati Ltd.), detecting the impact of particles on twelve stages and converting measured currents to total numbers of particles of the respective size range. Figure 5 shows the resulting particle size distribution for a typical ablation in air. In this example, a surface plane was processed with high-power laser pulses of 800 µJ. During all measurements, the majority of particles in the fume were clearly in the nanometer range: more than 90 % of the detected particles were smaller than 100 nm. When processing a surface which has already been roughened by previous ablation steps, particulate emission generally tends to increase, and the share of ultrafine particles below 100 nm clearly increases compared to the ablation of a blank surface. The mass of particulate matter below a size of 6 µm amounts to about 50 mg/min. For particles smaller than 100 nm, the mass rates are in the range of 400 µg/min.

It is therefore recommendable that during fs laser processes, such as microstructuring of zirconia ceramic, operators are efficiently protected from inhaling aerosols. Fine particles have a negligible settling velocity in air, so that efficient capture close to the source of emission is necessary to avoid contamination of the workplace [6].

The characteristics of the nanoparticles are also significantly influenced by the environmental medium. Previous investigations on nanoparticle formation have shown that the employment of water on the surface during the process

leads to smaller particles: The size fraction below 10 nm in the process emission clearly increases [11]. In gases, the choice of the environment is also relevant for the ablation mechanisms and the resulting process efficiency as well as emission characteristics. For example, the influence of the process gas on the particle size distribution has been studied for metals. During ablation of titanium, the majority of particles changes from a size around 100 nm to particles below 10 nm when using nitrogen instead of air [9]. It can be expected that nanoparticles from ceramic ablation show a comparable dependence on the atmosphere. However, microstructuring applications are usually restricted to normal atmosphere, as processing gas chambers are expensive. In other laser ablation applications, processing gas is also used to reduce heat generation in the work pieces. Due to the cold nature of ultrafast laser ablation, this is not an issue for dental crown machining from Y-TZP.

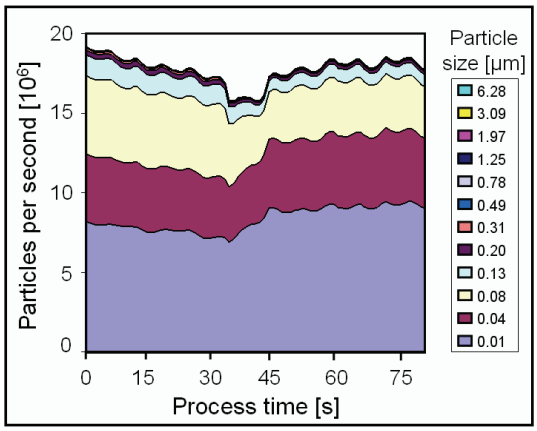

Figure 5: Particulate emission during ablation of Y-TZP, processing the same area twice using focused 800 µJ pulses at 1 kHz

In addition, it is obvious that the particles emerging from the surface will affect the ablation during subsequent laser pulses. Unless the pulse overlap is negligibly small, ablated particulate matter from the surface can lead to light scattering during subsequent laser pulses and to agglomerated matter on the surface and influence the further process.

2.3 Redeposition of debris

Debris results from particulate emission during the ablation process and significantly affects the quality of the generated surfaces. Figure 6 demonstrates such redeposition and agglomeration at the example of large pulse overlaps for low laser powers. For the left sample, the focus was placed on the sample surface, which is the common method for laser micromachining in air. The resulting material layer completely consists of solidified debris.

This layer is partly suppressable by varying process and laser parameters like feed rate, line pitch, pulse repetition rate, and focal position. It is known from literature that the speed of laser-ablated matter decreases exponentially from the workpiece surface. Even for typical initial particle velocities in the range of several 1000 m/s, speeds are close to zero when particles have reached a distance of several millimetres from the surface [3]. As a consequence, the emitted material falls back to the sample surface close to the place of ablation due to settling, or, if it is in the nanometre range (see section 2.2), stays airborne in close distance. In both cases, this material can agglomerate with ablated material from subsequent pulses. On the other hand, investigations on shock wave propagation (at the example of copper ablation with Q-switched Nd:YAG lasers) have shown velocities of more than 1000 m/s even in distances of more than 100 µm from the point of ablation [4].

In the case of the discussed sample, a slight variation of the focal plane position has been used to study this influence when using low pulse energies: the second sample in Figure 6 has been produced with a higher focal plane position. A focal shock wave above the surface is the supposed reason that prevents ablated material from remaining at its place and agglomerating to form a solid debris layer.

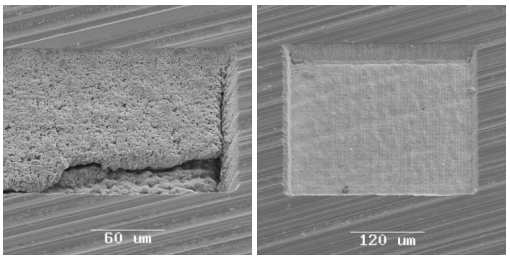

Figure 6: Debris effect using 10 µJ pulses and a 5 µm line pitch, focussing below (left) and above the surface (right)

Even for ablation which, on the macroscopic scale, seems debris-free, particulate matter from the ablation process can influence the macroscopic appearance: it causes a darkening of the sample due to an increased surface roughness. Figure 7 shows this behaviour at the example of lines that were generated by laser ablation with three different energies per section (applying varying processing speeds, i.e. varying pulse overlaps). EDX analyses of untreated ceramic blanks and structured samples prove that the fraction of oxygen at the surface of laser-processed samples does not decrease (with measured values even increasing from 58 to 62 atom %). This awareness excludes the possibility of metallic zirconia leading to the discolouration. In addition, the discolouration can be removed easily by heating the sample to above 300 °C for several minutes, which causes a sintering of micro- and nanoparticulate debris, diminishing the effect of light absorption from a rough surface formed by particulate matter.

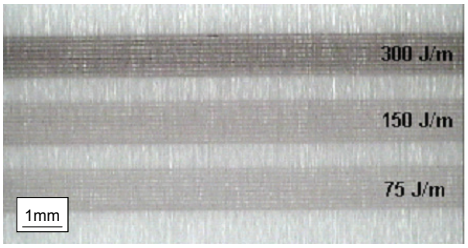

Figure 7: Photo of sample surface darkening in dependence of the line energy

3. Industrial processing station for dental crowns

Dental prostheses are characterised by complex three-dimensional free-form surfaces with structures on the 10 to 1000 µm scale. 3D machining must be applicable to almost all outer and inner surface areas, except for a residual pin connecting the ceramic blank with its mount. Relative movements between laser focus and workpiece are realised by the positioning system only. A laser scanner is not appli-

cable, since typical scribing speeds are four times lower than the specifications for this set-up, and interfacing of CNC axes and galvo scanner units is not yet state-of-the-art for real time processing. This has led to a design with a combination of stages whose dynamics shall be increased beyond the state-of-the-art of simultaneous five-axes machining. The required dynamics with regard to acceleration, deceleration and velocities result from the employment of ultrafast lasers with pulse repetitions up to 50 kHz. In order to control pulse overlapping (see section 2.1), the time for positioning movements must be kept short. Thus, necessary accelerations of 100 m/s² for the linear stages and 18 000 °/s² for the rotational stages of a turn-and-swivel unit have been determined. This is realised by light weight construction for all moving parts and by direct drives (ironless linear and torque motors). In addition, a high-speed CNC with shortest control loop cycles must be applied. The axes need a high mechanical stiffness to withstand the accelerations while keeping mechanical tolerances in the micron range. Stiffness is also important to avoid resonances and vibrations below 200 Hz. Figure 8 shows a sketch and a first real prototype.

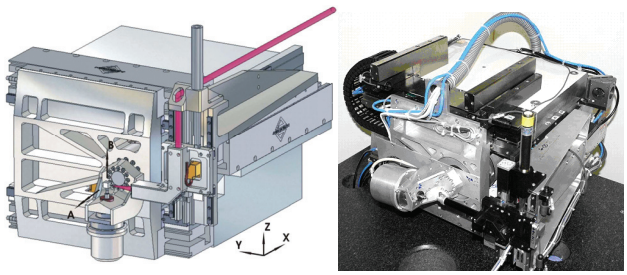

Figure 8: Five-axes positioning module with three linear and two rotational axes

One of the further constructional requirements is a completely closed housing (according to Machine Directive 98/37/EG and Laser Safety Standard EN ISO 60825-1), protecting operators against hazards from radiation, machine movements, and particulate process emission [11, 12]. Figure 9 shows the complete set-up containing machining module and laser system and the integration with all control elements in one housing. The machining space is encapsulated by a separate cabin with a fume extraction using filters for micro- and nanoparticulate process emissions. Besides health risks to operators, this reduces diffusion into the backspace of the machine where guidances and optical elements could be affected.

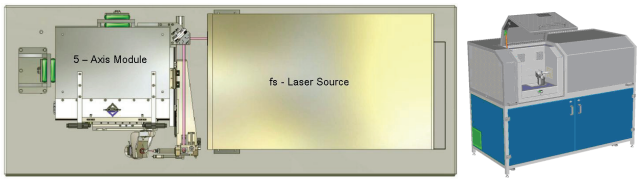

Figure 9: Left: Top view of 5-stage positioning module and laser head on granite base plate. Right: Housing with separate machining cabin and fume extraction

Using this machine layout and a 15 W fs laser system, a full-ceramic single crown will be machined from a 1 cm³ ceramic blank within about 1 hour. Only minor manual finishing work is needed at the spot of the mounting pin. Therefore, this manufacturing method will be more cost-effective than established methods for all-ceramic crowns.

4. Improvement of cement adhesion to zirconia

Since fixation of cements to ceramic substrates is mostly based on mechanical locking, the propagation of forces plays a major role for the surface design. To evaluate the influence of different microstructures, simulations on the behaviour of a simple system of dentin, cement, and ceramic have been performed. As indicated in Figure 10, this system has two parallel transition surfaces, of which the cement/ceramic transition is equipped with microstructures for an analysis of internal stresses.

This investigation calculates the effect of basic external forces that are usually in the range of up to 200 N. According to literature, the values for the material characteristics of the three phases were 18, 20, and 70 · 10^9 Pa for Young's modulus of dentin, cement, and ceramic, and Poisson's ratios of 0.31, 0.35, and 0.28, respectively [10, 13]. The width of the ceramic layer as well as the additional height of the microgrooves were set to 50 µm, which is a typical value for the gap width of dental restorations. In their total dimensions, the assumed ceramic and dentin block cross-sections were 6 mm wide and (each) 3 mm high.

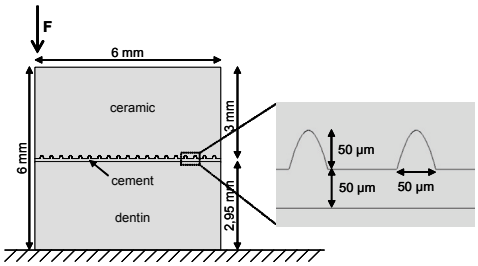

Figure 10: Sketch of a simulated 3-phase system with grooves

When applying a force to the upper left corner of this system in vertical direction, the resulting stress distribution reveals minor stress displacements along the transition surface and some peaks of high stress. This is especially relevant for the microgrooves on the left side close to the level of the external force vector. Figure 11 shows the resulting stress distribution for a simulated part that is equipped with such microstructures, and a detail of the transitions for the first two microgrooves on the left side, that are subject to the highest stress. According to this calculation, the resulting forces on the ceramic groove walls lead to stresses between 0.2 and 0.5 MPa, while the load on the cement is only in the range from 0.15 to 0.3 MPa. The peak stress is found to appear in the corner of the first microgroove in the ceramic. It is four orders of magnitude below critical values for the compression strength of Y-TZP of about 200 MPa.

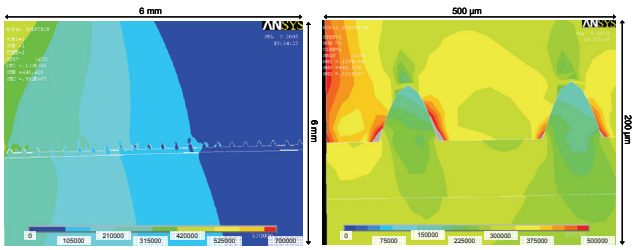

Figure 11: Stress simulation for F = 200 N and detail for the first two microgrooves on the left side

Based on the simulated geometries, the adhesive strength of such structures has been compared using shear and tensile stress tests. Samples have been structured with grooves of different widths as shown in Figure 12, that enable dental cements to fill the cavity during the fixation process.

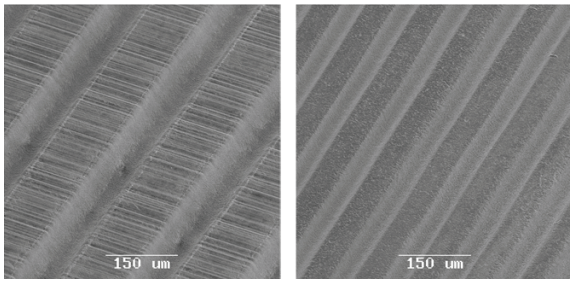

Figure 12: Sample ablation lines with an aspect ratio of 1 and line widths of 100 µm (left) and 50 µm (right)

Samples with such microshapes have been glued to each other as shown in Figure 13 and Figure 14 to apply shear and tensile forces. Due to the available sample shapes and testing equipment and for a better comparability with real-life shear and tensile forces, the measurements were not performed according to normed procedures [14, 15], but on the basis of the sketched sample alignments, still allowing a comparison with identical samples with no or different surface treatment.

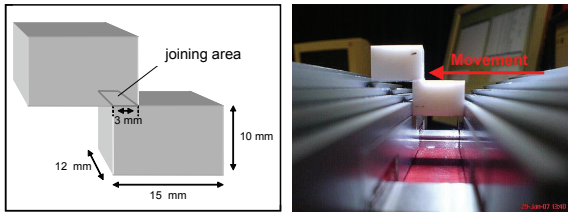

Figure 13: Test sample geometry of joined ceramic blanks and sample fixation for shear tests

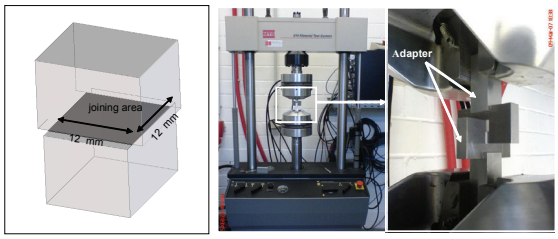

Figure 14: Geometry of joined blanks, tensile test set-up

Shear tests have been performed using a multifunctional bond-testing system, moving a sensor needle against the upper sample (above the fixation area) with a testing velocity of 50 µm/s as indicated in Figure 13. The measured shear stresses at the moment of breaking showed the strongest adhesion for a chemically adhesive composite (applying the product "Panavia"). Cement fixation using a merely adhesive composite ("Calibra") generally resulted in the weakest adhesion. Figure 15 shows that in the case of Panavia, a preparation of the ceramic surface with microgrooves in the size range of 50 µm leads to an increase in bonding strength by about 30 % in comparison with unconditioned surfaces. Even in the case of conventional sandblasting to increase the surface roughness, the applied shear forces were up to 20 % higher for the samples with microstructures.

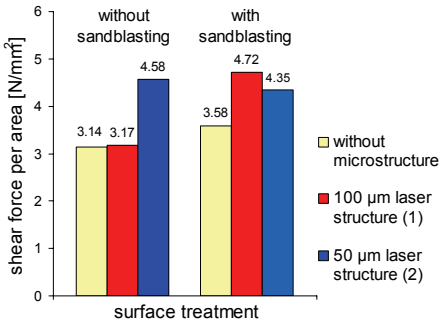

Figure 15: Shear stress for Y-TZP samples with and without laser-generated microstructures using "Panavia" for fixation

For the tensile tests, a standard machine with a custom-built adapter has been used, applying forces that were mostly in the range between 1 and 3 kN to separate the prepared samples. The resulting tensile strengths for samples that were fixed with Panavia are summarised in Figure 16. The increase of strength by the generation of linear microstructures amounted to values in the range of 100 %. In combination with conventional sandblasting, the increase of the necessary tensile forces was even higher (> 140 %).

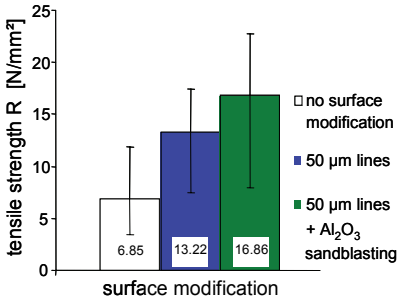

Figure 16: Tensile strength test results for Y-TZP using an adhesion with "Panavia" for non-modified and structured surfaces

The SEM pictures of the fractured surfaces in Figure 17 show that the microstructures were in fact well filled with cement, but that the breaking plane appears along the unstructured part of the ceramic, showing that the unconditioned parts of the surface contribute to the lower strength and initiate the break in these areas of low adhesion. Therefore, all parts of the surface should be included in the microstructuring process to increase adhesion values to a maximum.

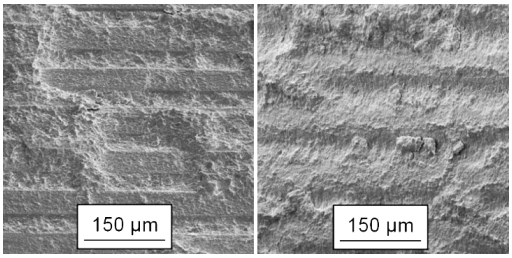

Figure 17: SEM pictures of fractured surfaces after tensile tests using a sample with microstructures without sandblasting (left) and a microstructured and sandblasted sample (right)

5. Summary and outlook

Y-TZP, one of the hardest ceramics, can be machined precisely and reproducibly using ultrafast lasers. The influence of the pulse overlap on the resulting surface quality can be traced back to micro- and especially nanoparticulate emission from the workpiece surface that influences subsequent ablation processes in the case of large pulse overlaps.

Using optimised laser ablation strategies, a machine design with dynamics beyond the state-of-the-art, and a femtosecond laser source with a repetition rate of up to 50 kHz and pulse energies of up to 300 µJ, a full-ceramic single crown is planned to be machined from a 1 cm^3 ceramic blank within about 1 hour, which makes this method more cost-effective than established methods.

The adhesion to dental cement can be significantly enhanced with the help of microstructures provided by an inner-surface laser structuring step at the end of the crown production. This increases the adhesion in non-structured surface areas and makes an additional sandblasting procedure unnecessary.

Acknowledgment

The authors acknowledge financial support by the German Federal Ministry of Education and Research (BMBF) within the joint project "forceramus" (reference numbers: 13N8553, 13N8556).

References

[1] P. Weigl, A. Kasenbacher, K. Werelius, *Dental Applications*, in F. Dausinger, F. Lichtner, and H. Lubatschowski (eds.), Femtosecond Technology for Technical and Medical Applications, Springer Topics in Appl. Phys. 96, 167 (2004).

[2] K. Werelius, P. Weigl: *Precise machining of ceramic dental prostheses with ultra-short laser pulses using online depth profiling.* Proc. PICALO 1 (2004)

[3] R. Dierken: *Untersuchungen zur Entstehung von Emissionen bei der Laserstrahlmaterialbearbeitung und deren Entfernung bei abtragenden Verfahren*. Thesis, Erlangen-Nürnberg, 1996.

[4] D. Jang, B. Oh, D. Kim, *Visualization of microparticle explosion and flow field in nanoparticle synthesis by pulsed laser ablation*, Appl. Phys. A 79, 1149 (2004).

[5] D.-W. Lee, M.-D. Cheng, *Investigations of nanoparticle generation during surface decontamination by laser ablation at low fluence*, J. Aerosol Sci. 35, 1513 (2004).

[6] S. Barcikowski, N. Bärsch, A. Ostendorf, *Generation of nanoparticles during laser ablation – risk assessment of non-beam hazards during laser cleaning*, Proc. LACONA 6 (2005).

[7] J. Bunte et al., Secondary Hazards: Particle and X-Ray Emission, in: *Femtosecond Technology for Technical and Medical Applications*, in F. Dausinger, F. Lichtner, and H. Lubatschowski (eds.), Topics in Applied Physics 96, 309 (2004).

[8] P. J. A. Borm, W. Kreyling, *Toxicological Hazards of Inhaled Nanoparticles – Potential Implication for Drug Delivery*, J. Nanosci. Nanotech. 4, 521 (2004).

[9] S. Barcikowski, A. Hahn, B. Chichkov: *Nanoparticles as Potential Risk during Femtosecond Laser Ablation*, J. Laser Appl. 19, 2, 65 (2007).

[10] T. Dérand, *Stress analysis of cemented or resin-bonded loaded porcelain inlays*, Dental Materials **7**, 21 (1991).

[11] N. Bärsch et al.: *Femtosecond laser microstructuring of hot-isostatically pressed zirconia ceramic.* J. Laser Appl. 19, 2, 107 (2007)

[12] S. Barcikowski et al.: *Generation of nanoparticles during laser ablation - risk assessment of non-beam hazards during laser cleaning.* Proc. LACONA 6 (2005)

[13] A. Misra et al., *Micromechanical Analysis of Dentin/Adhesive Interface by Finite Element Method*, J. Biomed. Mat. Res. 70B, 56 (2004).

[14] K. Eichner, H. F. Kappert, *Zahnärztliche Werkstoffe und ihre Verarbeitung*, Thieme Verlag, 6. Auflage, 1996

[15] A. S. Schinker, *Vergleich der Verbundfestigkeit unterschiedlicher Verblendkunststoffe auf verschiedenen Legierungen im Drei-Punkt-Biegeversuch*, Dissertation, Justus-Liebig-Universität Gießen, 2001

[16] A. Ostendorf, C. Kulik, T. Bauer, N. Bärsch, *Ablation of metals and semiconductors with ultrashort-pulsed lasers: improving surface qualities of microcuts and grooves,* Proc. SPIE 5340, 153 (2004).

[17] H. K. Tönshoff, A. Ostendorf, T. Wagner: *Structuring Silicon with femtosecond lasers,* Proc. SPIE 4274, 88 (2001)

(Received: May 12, 2007, Accepted: January 21, 2008)